Journal of Materials Chemistry A

COMMUNICATION

View Article Online
View Journal | View Issue

Cite this: J. Mater. Chem. A, 2016, 4, 8566

Received 30th April 2016
Accepted 9th May 2016

DOI: 10.1039/c6ta03605h

www.rsc.org/MaterialsA

One-dimensional (1D) [6,6]-phenyl-C_{61}-butyric acid methyl ester (PCBM) nanorods as an efficient additive for improving the efficiency and stability of perovskite solar cells†

Chenxin Ran,[a] Yonghua Chen,‡[b] Weiyin Gao,[a] Minqiang Wang*[a] and Liming Dai*[b]

We report a novel one dimensional (1D) [6,6]-phenyl-C_{61}-butyric acid methyl ester (PCBM) nanorod material as an efficient additive to form a wrinkle-like bicontinuous perovskite layer, where 1D PCBM nanorods can distribute homogenously throughout the film with an enlarged grain size. The resultant interconnected 1D PCBM nanorod within the perovskite material can also efficiently facilitate the photogenerated charge separation and carrier transportation process. An improved solar cell performance, from 9.5% up to 15.3%, was achieved using the optimized 1D PCBM nanorod content, along with enhanced device working stability. This work gives a new insight towards designing high performance organic–inorganic perovskite solar cells.

Introduction

Since 2012, organic–inorganic halide perovskite solar cells, mainly based on $CH_3NH_3PbX_3$ materials (X = Cl, Br, I), have become the most significant development in the field of solar cells.[1] This is because the $CH_3NH_3PbI_3$-based materials possess multiple advantages, including (i) strong and broad range of visible light absorption; (ii) ambipolar transport of electrons and holes; (iii) high charge mobility; (iv) small exciton binding energy, and (v) long exciton diffusion length.[2] Consequently, the power conversion efficiency (PCE) of the $CH_3NH_3PbX_3$ perovskite solar cells has rapidly exceeded 15% within two years,[3] followed by further improvement of PCE up to ~18%,[4–12] and the highest efficiency has exceeded over 20% in 2015.[7,12] Very recently, a certificated PCE of 15% has been reported for perovskite solar cells with a large aperture area >1 cm^2, showing potential for large-scale commercialization.[13] However, it is highly desirable to further enhance the PCE and stability of perovskite solar cells for specific practical applications.

To improve the performance of perovskite solar cells, most state-of-the-art studies have paid much attention to interface engineering,[4,5] compositional optimization,[12,14–19] solvent selection,[20–22] and device fabrication.[23–25] Of particular interest, certain small molecules, such as fullerene derivatives (*e.g.* PCBM, $A_{10}C_{60}$),[26–28] Lewis bases such as thiophene and pyridine,[29,30] and halogen-bonded supermolecular complexes,[31] have been used to successfully passivate the interface trap states at the grain boundaries by forming continuous pathways for charge carriers within the perovskite film. Among these materials, PCBM has already been widely used as an electron acceptor and electron transport layer in organic solar cells. Recently, one-dimensional (1D) PCBM nanorods have been successfully synthesized by a solution-based method.[32] Compared to C_{60} nanorods,[33,34] these newly developed 1D PCBM nanorods have even a higher surface area and transport channels with higher electron mobility. They are predicted to be ideal acceptor materials in organic solar cells.[32]

Herein, we report a significantly improved performance for $CH_3NH_3PbI_3$ perovskite solar cells by blending a small amount of 1D PCBM nanorods (typically 0–960 μg mL^{-1}) within the PbI_2/CH_3NH_3I (MAI) precursor solution in DMF (1.2 M, 0.208 mL) during the device fabrication (*vide infra*). Our results showed that the 1D PCBM nanorods can help forming a bicontinuous morphology and bulk-heterojunction structure through the thickness of the perovskite film, which can (i) enlarge the perovskite grain size, (ii) induce a large interfacial contact area between the PCBM nanorod and perovskite matrix, and (iii) improve the charge carrier separation and transportation within the perovskite film. As a result, the newly developed perovskite solar cell with the PCBM nanorod additive exhibited an enhanced PCE of 15.3%, compared with 9.5% for its counterpart without any additive, along with an increased open-

[a]Electronic Materials Research Laboratory, Key Laboratory of Education Ministry & International Center for Dielectric Research, Xi'an Jiaotong University, Xi'an, Shaanxi 710049, P. R. China. E-mail: mqwang126@126.com

[b]Center of Advanced Science and Engineering for Carbon, Department of Macromolecular Science and Engineering, Case Western Reserve University, Cleveland, Ohio 44106, USA. E-mail: lxd115@case.edu

† Electronic supplementary information (ESI) available. See DOI: 10.1039/c6ta03605h

‡ Present address: Key Laboratory of Flexible Electronics (KLOFE) & Institution of Advanced Materials (IAM), Jiangsu National Synergetic Innovation Center for Advanced Materials (SICAM), Nanjing Tech University (NanjingTech), 30 South Puzhu Road, Nanjing, Jiangsu, 211816, P. R. China.

circuit voltage (V_{OC}, from 0.74 to 0.90 V) and fill factor (FF, from 0.57 to 0.74), but with no photocurrent hysteresis.

Results and discussion

We used a simple and efficient liquid–liquid interfacial precipitation (LLIP) method reported recently[32] to synthesize the 1D PCBM nanorods. Briefly, PCBM nanosheets were first formed at the interface between the chloroform and methanol phases in a PCBM solution. Then, the interface was strongly disturbed by ultrasonication, and brown aggregated precipitates appeared at the bottom after standing for 24 h (Fig. S1†). After another 30 min sonication, 1D PCBM nanorods formed by folding the preformed PCBM nanosheets.[32] Fig. 1a shows TEM images of the pristine PCBM powder with random sphere morphology. After interface assembling by the LLIP method, PCBM molecules arranged into sheets as shown in Fig. 1b. Further ultrasonication of the PCBM sheets resulted in scroll-like PCBM nanorod structures. The HRTEM image given in Fig. 1d shows an individual scrolled PCBM nanorod with a diameter of ~10 nm, and length of 100–400 nm (Fig. 1c), which depends on the size of the PCBM sheets. The corresponding low magnification SEM images of 1D PCBM nanorods compared with PCBM sheets (Fig. S2†) demonstrated that most PCBM sheets scrolled up into the nanorod structure. From the XRD pattern in Fig. S2,† we can see that the assembling of PCBM powder into sheets led to a new distinct peak at ~6.0°, whose intensity is further enhanced after the scroll of PCBM sheets. From the theoretical calculation,[32] this new peak originated from the stacking of PCBM bilayer sheets, which have an intermolecular distance of ~15 Å, corresponding to the XRD peak at ~6.0°. After being scrolled into 1D PCBM nanorods, the overlapping of PCBM bilayer sheets resulted in an enhanced XRD peak intensity (red curve in Fig. S3†). Moreover, the produced 1D PCBM nanorods showed similar optical property with respect to the pristine PCBM powder (Fig. S4†), indicating that the PCBM molecular structure was not affected during the self-assembling LLIP method and the sonication process.

The effect of 1D PCBM nanorods on the properties of $CH_3NH_3PbI_3$ perovskite film was then characterized. It was found that the PbI_2/MAI precursor with 1D PCBM nanorods could form a homogeneous dispersion that was light brown in colour (Fig. 2a), which can be cast into uniform perovskite films. UV-Vis spectroscopic measurements (Fig. 2b) showed that the perovskite film with 1D PCBM exhibited higher absorption ability in the range from 550 nm to 750 nm, and different absorption behaviour in the infrared range compared with the control film without any additive, due to the thermodynamically favoured bonding of PCBM to defective halides, and this passivation effect is also beneficial for perovskite solar cell application.[26] Besides, it is observed that both films with or without 1D PCBM showed typical perovskite XRD peaks (Fig. 2c). Compared to the XRD pattern for the perovskite with no additive (Fig. 2c), the perovskite film with 1D PCBM nanorods exhibited relatively sharp and narrow peaks with a relatively small full width at the half maximum (FWHM) peak, suggesting the presence of highly crystallized perovskite particles with an enlarged grain size. Fig. 2d shows the PL spectra of the two perovskite films. It is well known that fullerenes and their derivatives are strong electron acceptors, and the C_{60} carbon core is able to accommodate even multiple electrons at the same time.[36] Here, a more striking PL quenching effect in the perovskite/1D PCBM composite film than that of the control perovskite film was clearly observed, which indicated that efficient photo-generated charge separation and extraction took place at the interface of the perovskite material and 1D PCBM nanorods. This PL quenching effect also indicates the large contact area between the perovskite and 1D PCBM nanorods.

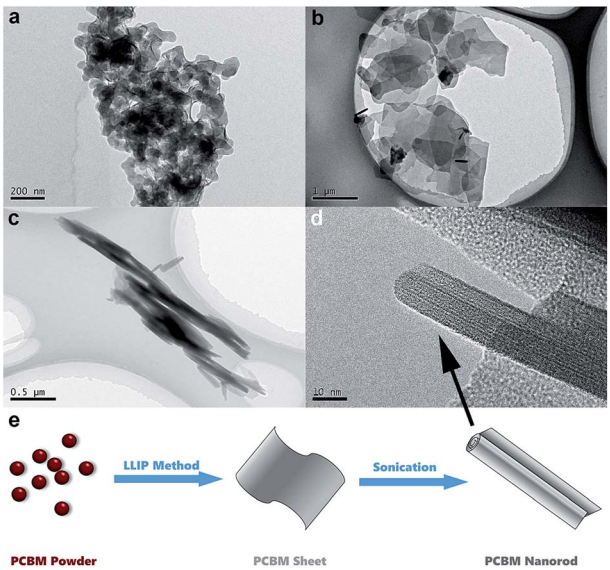

Fig. 1 TEM image of (a) pristine PCBM powder, (b) PCBM sheets produced by the LLIP method and (c) scroll-like PCBM nanorods after sonication. (d) HRTEM of 1D PCBM nanorods. (e) Schematic procedure for 1D PCBM nanorod formation.

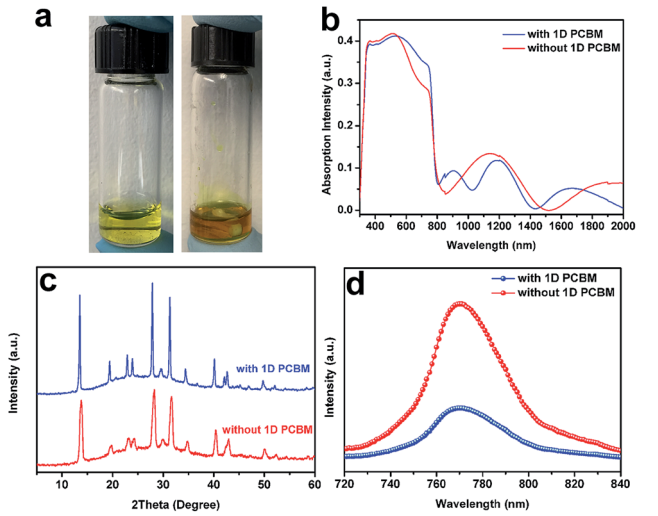

Fig. 2 (a) Digital images of PbI_2/MAI precursor solution (left) and PbI_2/MAI precursor solution with 240 μg mL^{-1} 1D PCBM nanorods (right). (b) UV-Vis, (c) XRD and (d) PL spectrum excitation at 470 nm of the corresponding perovskite film.

Morphologies of the films made from the PbI_2/MAI precursor with different 1D PCBM nanorod concentrations were further characterized. As shown in Fig. 3a–d, a uniform pinhole-free morphology with enlarged grain size was observed for all perovskite films as the 1D PCBM concentration of the precursor solution increased from 0 to 960 μg mL^{-1}. However, some pinholes and cracks appeared when the 1D PCBM content became too high (2400 μg mL^{-1}, Fig. 3e), though the grain size of the film kept increasing. The perovskite film without any additive showed a mean grain size of 180 nm with the smallest 40 nm and largest 510 nm (Fig. 3f, Table S1†). When a small amount of 1D PCBM (96 μg mL^{-1}) was added, the mean grain size increased up to 240 nm (Fig. 3f, Table S1†). Further increasing the content of 1D PCBM nanorods resulted in an enlarged grain size of the perovskite film, which is in agreement with the XRD result above (Fig. 2c). The direct proportional relationship between the 1D PCBM content and the grain size of the perovskite film shown in Fig. 3f–j and S5† implies that the addition of 1D PCBM nanorods during the perovskite film formation can significantly affect the crystalline process to increase the perovskite grain size and reduce the grain boundaries. The enlarged grain size may originate from the anisotropy of rod-like shaped 1D PCBM during the spin coating process. In contrast, addition of the pristine PCBM powder did not cause an increase in the grain size of the perovskite film (Fig. S6†), which is consistent with the work using PCBM as an additive.[26,27] Besides, the films with 1D PCBM nanorods showed a wrinkle-like surface morphology (Fig. 3b–e). Moreover, the cross-section SEM images in Fig. 4a–c show that a bicontinuous composite structure can be formed within the whole thickness of the perovskite film with 1D PCBM nanorods with respect to the control perovskite film with no additive. Previous studies using PCBM powder as an additive didn't show such a unique morphology and enlarged grain size, for either the one-step fabrication of $CH_3MH_3PbI_3$/PCBM film[26] or two-step fabrication of PbI_2-PCBM film.[27] Besides, different from the obvious strip-like morphology in this work (Fig. 3e), when excess PCBM powder in the film was used in both previous studies, a spherical particle-shaped aggregation phase was observed,[26,27] demonstrating the important role of 1D PCBM nanorods as an additive in $CH_3NH_3PbI_3$ film formation.

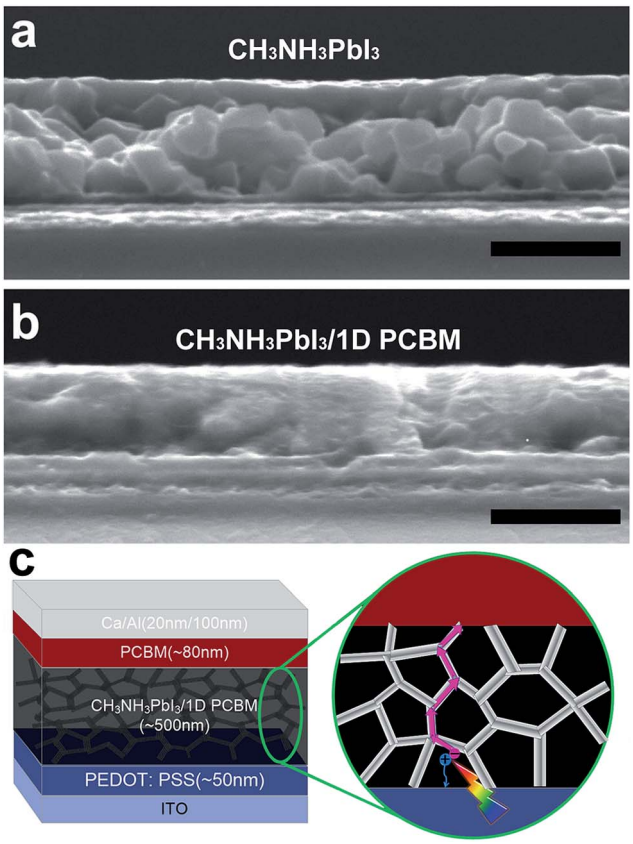

Fig. 4 Cross-section SEM image of the (a) $CH_3NH_3PbI_3$ and (b) $CH_3NH_3PbI_3$/1D PCBM nanorod film. (c) Scheme of a planar perovskite solar cell using 1D PCBM nanoribbons as the additive. Scale bar: 0.5 μm.

It is well known that a larger perovskite grain size is beneficial to the improvement of the solar cell performance because

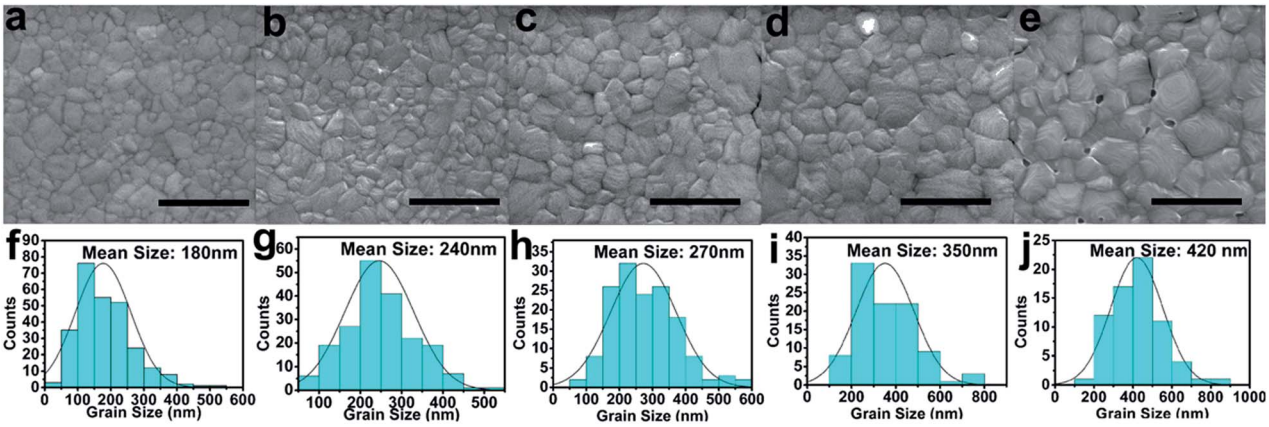

Fig. 3 SEM images of perovskite films with increasing content of 1D PCBM nanorods as additives: (a) 0 μg mL^{-1}, (b) 96 μg mL^{-1}, (c) 240 μg mL^{-1}, (d) 960 μg mL^{-1}, and (e) 2400 μg mL^{-1}. Scale bar: 1 μm. (f–j) The corresponding histograms of the grain size distribution of the five perovskite films, inset shows the mean grain size of the film.

a larger grain size can lead to (i) a reduced interfacial area between the perovskite grains and suppressed charge trapping to eliminate hysteresis, and (ii) a lower bulk defect density and higher carrier mobility, allowing for the photogenerated charge carriers to be transported through the perovskite layer without frequent encounters with defects and impurities.[4] Furthermore, the homogeneous appearance of the wrinkle-like morphology on the surface of the perovskite particles (Fig. 3b–e) as well as within the perovskite film (Fig. 4b) indicates that the 1D PCBM nanorods not only cover the perovskite grains to enlarge the interface between the perovskite material and 1D PCBM nanorods, but are also distributed uniformly through the thickness to form a bicontinuous bulk heterojunction structure, which greatly benefits the charge separation and transportation process.

A recent theoretical study has shown that PCBM could bind to iodide-rich defect sites,[26] which explains both the observed close binding between 1D PCBM nanorods and the $CH_3NH_3PbI_3$ structure as well as the homogeneous distribution of 1D PCBM nanorods in the perovskite matrix to form a bulk-heterojunction structure. Similar to other inorganic polycrystalline solar cells, such as silicon, cadmium telluride (CdTe), and copper indium gallium selenide (CIGS) solar cells,[37] passivating the dangling bonds in the polycrystalline solar cells, which caused a large density of 'surface states' in the band gap, is one of the essential methods to minimize the charge recombination at the perovskite material surface.[38] Therefore, the unique morphology changes induced by the addition of the 1D PCBM nanorods are expected to have a positive impact on the performance of perovskite solar cells. We then used a simple one-step method to fabricate the $CH_3NH_3PbI_3$ perovskite solar cells (see the Experimental section for the details of device fabrication). Fig. 4c schematically shows the device structure for a typical perovskite solar cell developed in this study.

By introducing an increasing amount of 1D PCBM nanorods into the light absorbing layer within the perovskite solar cells (*cf.* Fig. 4c), we observed an enhancement in the photovoltaic performance with respect to its counterpart without any additive. Mixed light absorbing layers with different amounts of 1D PCBM nanorods were prepared by dispersing different amounts of 1D PCBM solution (0–200 μL, 1 mg mL^{-1} in DMF) into 1.2 M PbI_2/MAI (115 mg/40 mg) precursor solution to form a homogeneous mixture solution with the final concentration of 1D PCBM from 0 μg mL^{-1} to 960 μg mL^{-1}. As shown in Fig. S7,† all the solar cells containing the 1D PCBM nanorods showed an enhancement of the PCE compared to the control device without any additive. Table 1 lists the numerical results from Fig. S7.† It is worth noting that the performance of the perovskite solar cells first increased with increasing content of the 1D PCBM nanorods up to about 240 μg mL^{-1}. Further increase in the 1D PCBM nanorods content caused a decrease in the solar cell performance. More specifically, the PCE initially increased from 9.54% to 14.34% as the content of 1D PCBM nanorods increased from 0 to 240 μg mL^{-1}, and further addition of the 1D PCBM nanorods up to 960 μg mL^{-1} reduced the PCE to 11.48%. The control device prepared under the same conditions, but without any additive, showed a PCE of 9.5% only. Here, the concentration of PbI_2/MAI is 1.2 M and the thickness of the film is ~500 nm, which is too thick to achieve high performance for the pure $CH_3NH_3PbI_3$ device, as demonstrated by others.[3,25,35,39,40] The curves of V_{OC}, J_{SC}, FF and PCE as a function of the content of 1D PCBM nanorods given in Fig. S8† all show a similar optimum content of the 1D PCBM nanorods around 240 μg mL^{-1} for the best performing device. The values of V_{OC} and FF highly depend on the quality of the $CH_3NH_3PbI_3$ film. High film quality requires a dense and continuous film structure as well as high crystallinity of the film, and any factor that lowers the film quality will lead to decreased V_{OC} as well as FF. Before optimization of the 1D PCBM nanorods content, the increased V_{OC} was due to improved perovskite film quality (highly crystalline, low defect and large grain size) while the increased FF originated from the positive effect of 1D PCBM nanorods on the charge separation and transportation within the perovskite film, but further increasing the content of 1D PCBM nanorods over the optimized dosage sacrificed the quality of the film, leading to both decreased V_{OC} and FF. However, J_{SC} showed little change with increasing content of the 1D PCBM nanorods resulting from a counterbalance between the following two opposite effects: (i) photoinduced charge transfer was increasingly more impeded when V_{OC} increased;[41] (ii) 1D PCBM nanorods facilitated the charge transportation process to increase J_{SC}. Based on the above experimental observations, we envision that a continuous network of the 1D PCBM nanorods forms at the optimum 1D PCBM content (*i.e.*, 240 μg mL^{-1}) *via* a percolation threshold process, and that further increase in the 1D PCBM content above the percolation

Table 1 Performance parameters of perovskite solar cells with different 1D PCBM additions[a]

1D PCBM concentration (μg mL^{-1})	V_{OC} (V)	J_{SC} (mA cm^{-2})	FF	PCE (%)
0	0.74 ± 0.01	22.49 ± 0.18	0.57 ± 0.01	9.54 ± 0.29
48	0.76 ± 0.01	22.98 ± 0.20	0.61 ± 0.02	10.55 ± 0.34
96	0.85 ± 0.01	21.80 ± 0.22	0.66 ± 0.02	12.28 ± 0.29
240	0.89 ± 0.01	22.43 ± 0.24	0.74 ± 0.01	14.34 ± 0.38
480	0.81 ± 0.02	22.02 ± 0.28	0.68 ± 0.02	12.18 ± 0.27
960	0.78 ± 0.02	21.51 ± 0.27	0.69 ± 0.02	11.48 ± 0.31
240 (PCBM)	0.87 ± 0.02	18.93 ± 0.20	0.74 ± 0.01	12.59 ± 0.22

[a] Average and standard deviation values were obtained based on 8 cells for each of the data.

threshold does not lead to any obvious further increase in the pathways for charge transportation, but a significant reduction in the active perovskite material and its associated light absorbance, along with a concomitant morphology change of the perovskite phase (*cf.* Fig. 3e).

Fig. 5a shows the *J–V* curve of the best performing cell obtained by further optimizing the $CH_3NH_3PbI_3$ perovskite solar cell with 240 μg mL^{-1} of the 1D PCBM nanorods, which exhibited a high J_{SC} of 22.88 mA cm^{-2}, V_{OC} of 0.90 V, and FF of 0.743, resulting in a PCE of 15.30%. Furthermore, this device showed negligible hysteresis (Fig. 5b) as the fullerene based materials could effectively passivate charge traps in perovskite materials to eliminate the notorious photocurrent hysteresis.[38] The incident photon-to-current efficiency (IPCE) was high over the whole visible-light range with a maximum value close to 85% around 490 nm (Fig. 5c), and the J_{SC} value integrated from the IPCE spectrum was found to be in good agreement with that measured from the *J–V* curve (*i.e.*, 22.88 mA cm^{-2}).

We also compare the performance of the best device with that of its counterpart with the pristine PCBM powder as an additive at the same concentration (240 μg mL^{-1}) in Table 1. As shown in Fig. 5d, the best performing device using the pristine PCBM powder as the additive showed a J_{SC} of 19.04 mA cm^{-2}, V_{OC} of 0.88 V, FF of 0.75, and PCE of 12.57%. Most of these values are better than those of the control device without any PCBM (*cf.* Fig. S7†), but worse than the corresponding values for the perovskite solar cells using the optimized content of 1D PCBM nanorods as the additive, indicating, once again, that the addition of the 1D PCBM nanorods with an increased grain size and unique continuous structure could significantly improve the solar cell performance.

The stability of the perovskite solar cells under device working conditions is one of the most important issues that need to be tested for practical applications.[42] In this regard, we have also characterized the photostability of unencapsulated perovskite solar cells fabricated with and without the addition of 1D PCBM nanorods under continuous simulated sunlight irradiation in air at room temperature (room humidity: 30 ± 1%RH). Since a Ca/Al cathode is not stable in air, we used Ag as the cathode for testing the photostability of the perovskite solar cells in air, though the performance using the Ag cathode decreased a little compared with that of the Ca/Al cathode (Fig. S9†). As can be seen in Fig. 6, the perovskite solar cell with 1D PCBM nanorods showed enhanced stability over 3600 s continuous simulated sunlight irradiation compared with its counterpart without any additives. Fig. 6a and c indicate that the improved stability is mainly owing to the reduced decay of J_{SC} and FF during the test while the V_{OC} didn't show any decay (Fig. 6b) for perovskite solar cells either with or without the 1D PCBM additive.

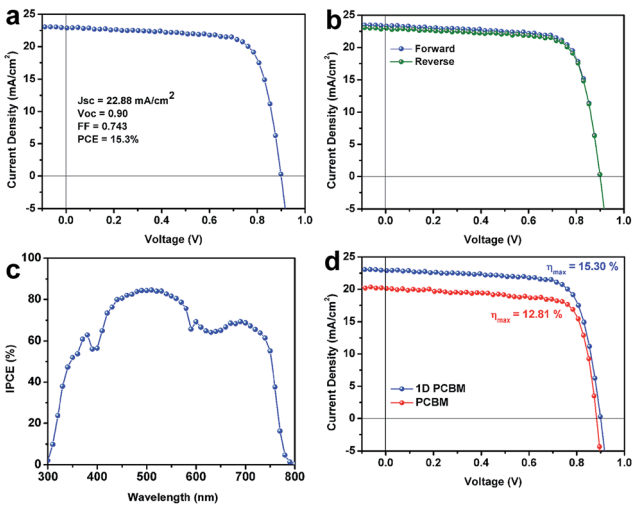

Fig. 5 (a) *J–V* curves for the best performing device. (b) *J–V* curves obtained for different bias scan directions: from forward to reverse (blue) and from reverse to forward (green). (c) IPCE spectrum of the best performing device. (d) *J–V* curves of the device using 1D PCBM (blue) and PCBM (red) as the additives, respectively.

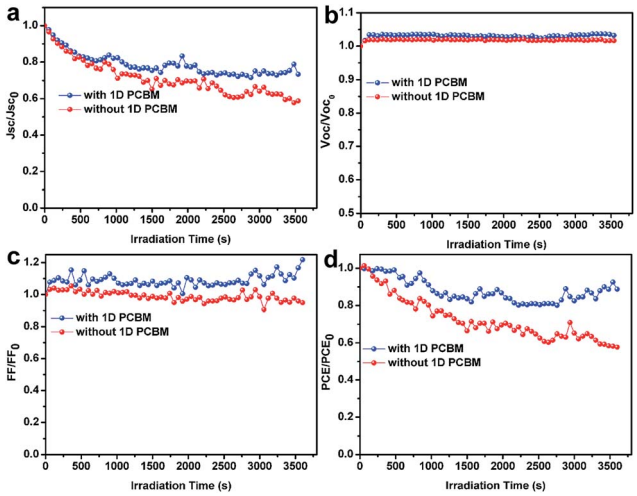

Fig. 6 (a) J_{SC}, (b) V_{OC}, (c) FF and (d) PCE variations of the perovskite solar cells fabricated with and without 1D PCBM nanorod additives under continuous simulated sunlight irradiation.

Previous studies have indicated that water permeates the perovskite crystal along the grain boundaries to cause gradual degradation of the film.[43,44] Thus, it is reasonable for us to believe that the improved photostability we observed in this study is caused by the reduced grain boundaries upon the introduction of the 1D PCBM nanorods. It has also been reported that the photostability of certain organic fluorescence semiconductors can be improved using carbon-based additives, such as fullerenes,[45] graphene or graphene composites,[46,47] and carbon nanotubes,[48] through the efficient photo-charge transfer effect, as also indicated by the PL quenching associated with the addition of the 1D PCBM nanorods into the $CH_3NH_3PbI_3$ perovskite film in this study (Fig. 2d). Besides, the above-mentioned strong binding capability of PCBM to iodide-rich defect sites, which passivates the interface of the perovskite grains and hence the associated moisture adsorption, may have also contributed to the improved photostability of our perovskite solar cells.

Conclusions

In conclusion, we have demonstrated a significantly improved $CH_3NH_3PbI_3$ perovskite solar cell performance by using 1D

PCBM nanorods as an additive. It was found that the presence of scroll-like 1D PCBM nanorods can effectively enlarge the grain size of the perovskite film and form an interesting wrinkle-like morphology on the surface and through the thickness of the perovskite film, which increased the interface between the perovskite and 1D PCBM nanorods to facilitate charge separation. Moreover, the well-distributed 1D PCBM nanorods could form an interconnected bulk-heterojunction structure within a bicontinuous morphology, which provides an efficient charge transportation pathway for charge carriers. As a result, PCE as high as 15.3% and much improved device working stability have been obtained for the $CH_3NH_3PbI_3$ perovskite solar cell with an optimum amount of the 1D PCBM nanorods (240 μg mL^{-1}, Fig. 6). This work provides a new and efficient approach for enhancing the performance of perovskite solar cells. The methodology developed in this study is rather general and can be applied to many other solar cells.

Acknowledgements

This work has been financially supported by the 111 Program (No. B14040), Natural Science Foundation of China (Grant No. 51572216 and 61176056) and the NSFC Major Research Plan on Nanomanufacturing (Grant No. 91323303). The authors gratefully acknowledge financial support from the Industrial Science and Technology Research Project in Shaanxi province (2015GY005) and the open projects from the Institute of Photonics and Photo-Technology, Provincial Key Laboratory of Photoelectronic Technology, Northwest University, China. The authors also sincerely appreciate the support from the China Scholarship Council (CSC).

Notes and references

1 T. C. Sum and N. Mathews, *Energy Environ. Sci.*, 2014, **7**, 2518.
2 H. J. Snaith, *J. Phys. Chem. Lett.*, 2013, **4**, 3623.
3 M. Z. Liu, M. B. Johnston and H. J. Snaith, *Nature*, 2013, **501**, 395.
4 W. Y. Nie, H. H. Tsai, R. Asadpour, J. C. Blancon, A. J. Neukirch, G. Gupta, J. J. Crochet, M. Chhowalla, S. Tretiak, M. A. Alam, H. L. Wang and A. D. Mohite, *Science*, 2015, **347**, 522.
5 H. P. Zhou, Q. Chen, G. Li, S. Luo, T. B. Song, H. S. Duan, Z. R. Hong, J. B. You, Y. S. Liu and Y. Yang, *Science*, 2014, **345**, 542.
6 J. P. C. Baena, L. Steier, W. Tress, M. Saliba, S. Neutzner, T. Matsui, F. Giordano, T. J. Jacobsson, A. R. S. Kandada, S. M. Zakeeruddin, A. Petrozza, A. Abate, M. K. Nazeeruddin, M. Gratzel and A. Hagfeldt, *Energy Environ. Sci.*, 2015, **8**, 2928.
7 W. S. Yang, J. H. Noh, N. J. Jeon, Y. C. Kim, S. Ryu, J. Seo and S. I. Seok, *Science*, 2015, **348**, 1234.
8 J. H. Heo, H. J. Han, D. Kim, T. K. Ahn and S. H. Im, *Energy Environ. Sci.*, 2015, **8**, 1602.
9 C. Bi, Q. Wang, Y. C. Shao, Y. B. Yuan, Z. G. Xiao and J. S. Huang, *Nat. Commun.*, 2015, **6**, 7747.
10 N. Ahn, D. Y. Son, I. H. Jang, S. M. Kang, M. Choi and N. G. Park, *J. Am. Chem. Soc.*, 2015, **137**, 8696.
11 Q. F. Dong, Y. B. Yuan, Y. C. Shao, Y. J. Fang, Q. Wang and J. S. Huang, *Energy Environ. Sci.*, 2015, **8**, 2464.
12 N. J. Jeon, J. H. Noh, W. S. Yang, Y. C. Kim, S. Ryu, J. Seo and S. I. Seok, *Nature*, 2015, **517**, 476.
13 W. Chen, Y. Z. Wu, Y. F. Yue, J. Liu, W. J. Zhang, X. D. Yang, H. Chen, E. B. Bi, I. Ashraful, M. Gratzel and L. Y. Han, *Science*, 2015, **350**, 944.
14 G. E. Eperon, V. M. Burlakov, P. Docampo, A. Goriely and H. J. Snaith, *Adv. Funct. Mater.*, 2014, **24**, 151.
15 Y. X. Zhao and K. Zhu, *J. Am. Chem. Soc.*, 2014, **136**, 12241.
16 F. Wang, H. Yu, H. H. Xu and N. Zhao, *Adv. Funct. Mater.*, 2015, **25**, 1120.
17 Q. Chen, H. P. Zhou, Y. H. Fang, A. Z. Stieg, T. B. Song, H. H. Wang, X. B. Xu, Y. S. Liu, S. R. Lu, J. B. You, P. Y. Sun, J. Mckay, M. S. Goorsky and Y. Yang, *Nat. Commun.*, 2015, **6**, 7269.
18 N. Yantara, F. Yanan, C. Shi, H. A. Dewi, P. P. Boix, S. G. Mhaisalkar and N. Mathews, *Chem. Mater.*, 2015, **27**, 2309.
19 S. Dharani, H. A. Dewi, R. R. Prabhakar, T. Baikie, C. Shi, Y. H. Du, N. Mathews, P. P. Boix and S. G. Mhaisalkar, *Nanoscale*, 2014, **6**, 13854.
20 J. H. Noh, S. H. Im, J. H. Heo, T. N. Mandal and S. I. Seok, *Nano Lett.*, 2013, **13**, 1764.
21 N. J. Jeon, J. H. Noh, Y. C. Kim, W. S. Yang, S. Ryu and S. Il Seol, *Nat. Mater.*, 2014, **13**, 897.
22 Y. G. Rong, Z. J. Tang, Y. F. Zhao, X. Zhong, S. Venkatesan, H. Graham, M. Patton, Y. Jing, A. M. Guloy and Y. Yao, *Nanoscale*, 2015, **7**, 10595.
23 Y. H. Chen, T. Chen and L. M. Dai, *Adv. Mater.*, 2015, **27**, 1053.
24 M. Ramesh, K. M. Boopathi, T. Y. Huang, Y. C. Huang, C. S. Tsao and C. W. Chu, *ACS Appl. Mater. Interfaces*, 2015, **7**, 2359.
25 Z. G. Xiao, C. Bi, Y. C. Shao, Q. F. Dong, Q. Wang, Y. B. Yuan, C. G. Wang, Y. L. Gao and J. S. Huang, *Energy Environ. Sci.*, 2014, **7**, 2619.
26 J. Xu, A. Buin, A. H. Ip, W. Li, O. Voznyy, R. Comin, M. J. Yuan, S. Jeon, Z. J. Ning, J. J. McDowell, P. Kanjanaboos, J. P. Sun, X. Z. Lan, L. N. Quan, D. H. Kim, I. G. Hill, P. Maksymovych and E. H. Sargent, *Nat. Commun.*, 2015, **6**, 7081.
27 C. Chiang and C. Wu, *Nat. Photonics*, 2016, **10**, 196.
28 K. Wang, C. Liu, P. C. Du, J. Zheng and X. Gong, *Energy Environ. Sci.*, 2015, **8**, 1245.
29 D. W. deQuilettes, S. M. Vorpahl, S. D. Stranks, H. Nagaoka, G. E. Eperon, M. E. Ziffer, H. J. Snaith and D. S. Ginger, *Science*, 2015, **348**, 683.
30 N. K. Noel, A. Abate, S. D. Stranks, E. S. Parrott, V. M. Burlakov, A. Goriely and H. J. Snaith, *ACS Nano*, 2014, **8**, 9815.
31 A. Abate, M. Saliba, D. J. Hollman, S. D. Stranks, K. Wojciechowski, R. Avolio, G. Grancini, A. Petrozza and H. J. Snaith, *Nano Lett.*, 2014, **14**, 3247.

32 E. Gracia-Espino, H. R. Barzegar, T. Sharifi, A. M. Yan, A. Zettl and T. Wagberg, *ACS Nano*, 2015, **9**, 10516.
33 C. Larsen, H. R. Barzegar, F. Nitze, T. Wagberg and L. Edman, *Nanotechnology*, 2012, **23**, 1995.
34 H. R. Barzegar, C. Larsen, L. Edman and T. Wagberg, *Part. Part. Syst. Charact.*, 2013, **30**, 715.
35 M. D. Xiao, F. Z. Huang, W. C. Huang, Y. Dkhissi, Y. Zhu, J. Etheridge, A. Gray-Weale, U. Bach, Y. B. Cheng and L. Spiccia, *Angew. Chem., Int. Ed.*, 2014, **53**, 9898.
36 A. Abrusci, S. D. Stranks, P. Docampo, H. L. Yip, A. K. Jen and H. J. Snaith, *Nano Lett.*, 2013, **13**, 3124.
37 H. S. Kim, I. Mora-Sero, V. Gonzalez-Pedro, F. Fabregat-Santiago, E. J. Juarez-Perez, N. G. Park and J. Bisquert, *Nat. Commun.*, 2013, **4**, 375.
38 Y. H. Shao, Z. G. Xiao, C. Bi, Y. B. Yuan and J. S. Huang, *Nat. Commun.*, 2014, **5**, 5784.
39 D. Y. Liu, M. K. Gangishet ty and T. L. Kelly, *J. Mater. Chem. A*, 2014, **2**, 19873.
40 Z. G. Xiao, Q. F. Dong, C. Bi, Y. C. Shao, Y. B. Yuan and J. S. Huang, *Adv. Mater.*, 2014, **26**, 6503.
41 D. Di Nuzzo, G. J. A. H. Wetzelaer, R. K. M. Bouwer, V. S. Gevaerts, S. C. J. Meskers, J. C. Hummelen, P. W. M. Blom and R. A. J. Janssen, *Adv. Energy Mater.*, 2013, **3**, 85.
42 T. Leijtens, G. E. Eperon, N. K. Noel, S. N. Habisreutinger, A. Petrozza and H. J. Snaith, *Adv. Energy. Mater.*, 2015, **5**, 1500963.
43 J. A. Christians, P. A. M. Herrera and P. V. Kamat, *J. Am. Chem. Soc.*, 2015, **137**, 1530.
44 A. M. A. Leguy, Y. Hu, M. Campoy-Quiles, M. I. Alonso, O. J. Weber, P. Azarhoosh, M. van Schilfgaarde, M. T. Weller, T. Bein, J. Nelson, P. Docampo and P. R. F. Barnes, *Chem. Mater.*, 2015, **27**, 3397.
45 E. T. Hoke, I. T. Sachs-Quintana, M. T. Lloyd, I. Kauvar, W. R. Mateker, A. M. Nardes, C. H. Peters, N. Kopidakis and M. D. McGehee, *Adv. Energy. Mater.*, 2012, **2**, 1351.
46 C. X. Ran, M. Q. Wang, W. Y. Gao, J. J. Ding, Y. H. Shi, X. H. Song, H. W. Chen and Z. Y. Ren, *J. Phys. Chem. C*, 2012, **116**, 23053.
47 C. X. Ran, M. Q. Wang, W. Y. Gao, Z. Yang, J. P. Deng, J. J. Ding and X. H. Song, *Phys. Chem. Chem. Phys.*, 2014, **16**, 4561.
48 P. J. Goutam, D. K. Singh, P. K. Giri and P. K. Iyer, *J. Phys. Chem. B*, 2011, **115**, 919.

